

## Helicity of magnetic domains in holmium studied with circularly polarized x rays

C. Sutter, G. Grübel, and C. Vettier

*European Synchrotron Radiation Facility, Boîte Postale 220, F-38043 Grenoble Cédex, France*

F. de Bergevin

*Laboratoire de Cristallographie, CNRS, Boîte Postale 166, F-38042 Grenoble Cédex, France*

A. Stunault

*European Synchrotron Radiation Facility, Boîte Postale 220, F-38043 Grenoble Cédex, France*

Doon Gibbs

*Department of Physics, Brookhaven National Laboratory, Upton, New York 11973*

C. Giles

*Laboratorio Nacional de Luz Sincrotron, Caixa Postale 6192, 13081-970 Campinas, São Paulo, Brazil*

(Received 15 July 1996)

We have studied the helicity of magnetic domains in antiferromagnetic holmium using circularly polarized x rays. The spiral magnetic structure of holmium gives rise to pairs of magnetic satellites split symmetrically around each of the main charge Bragg reflections. For circularly polarized light the nonresonant scattering amplitudes at these satellites depend upon the helicity of the spiral, and thereby yield information about the distribution of magnetic domains with opposite helicity in the sample. The high degree of circular polarization (96%) in the incident beam was obtained by transforming a linearly polarized undulator beam with the help of a diamond quarter-wave plate. The data reveal that domains with opposite helicity were nearly equally distributed in the crystal under investigation. [S0163-1829(97)03901-5]

### I. INTRODUCTION

The polarization and resonance properties of the x-ray magnetic scattering cross section have been used successfully to elucidate the magnetic properties of rare earth, actinide, and transition metal systems. The polarization dependence of the nonresonant magnetic cross section was calculated by Blume and Gibbs<sup>1</sup> in 1988. They showed that the spin and orbital magnetization densities contribute linearly, but with different polarization dependencies to the cross section. This makes it possible not only to distinguish between charge and magnetic scattering but also to determine the spin ( $S$ ) and orbital angular ( $L$ ) momentum by measuring the polarization dependence of the x-ray magnetic scattering cross section. Pioneering experiments exploring the magnetic cross section with linearly polarized x rays were carried out in antiferromagnetic holmium<sup>2</sup> and uranium arsenide.<sup>3</sup> Substantial parts of the cross section depending upon the degree of circular polarization, however, remained largely unexplored experimentally due to the lack of intense sources for circularly polarized light. Among them are elastic interference scattering in ferromagnets [inelastic interference (Compton) scattering has been observed in several systems<sup>4</sup>] and the possibility of studying the helicity of spiral antiferromagnets. It has been predicted<sup>1</sup> that the circular components of the nonresonant cross section of the positive ( $+\tau$ ) and negative ( $-\tau$ ) satellites in a spiral antiferromagnet have opposite helicity in a simple spiral domain. A magnetic scattering experiment with circularly polarized x rays therefore allows direct determination of the distribution of domains

with opposite helicity. Circular polarization also gives access to the interference between charge and magnetic scattering (interference scattering), thus allowing magnetic scattering in ferromagnets to be studied without an external field.

Intense circularly polarized x-ray beams can be produced either by special insertion devices like asymmetric wigglers and helical undulators or by combining a planar undulator with an x-ray phase plate.<sup>5</sup> We have used a diamond phase plate to convert the linearly polarized radiation emitted by a planar undulator from the ESRF into left- and right-hand circularly polarized x rays with a degree of circular polarization of  $P_\eta = \pm 0.96$  to study the helicity of magnetic domains in antiferromagnetic holmium. More specifically, we have measured the nonresonant scattering intensity of the  $(00L \pm \tau)$  magnetic satellites (where  $\tau$  is the modulation wave vector and  $L=2,4,6$ ) for circularly polarized light of both helicities (left and right). Our results prove that magnetic domains of opposite helicity exist in the sample under investigation and were about equally distributed. The results are consistent with previous neutron topography studies<sup>6</sup> on holmium and show that nonresonant magnetic x-ray scattering with circularly polarized light can reveal valuable information about the helicity and distribution of spiral domains in antiferromagnets.

### II. EXPERIMENTAL DETAILS

The experiments were performed at beamline 9/ID10 (Troika) of the European Synchrotron Radiation Facility (ESRF). A schematic layout of the experimental setup is

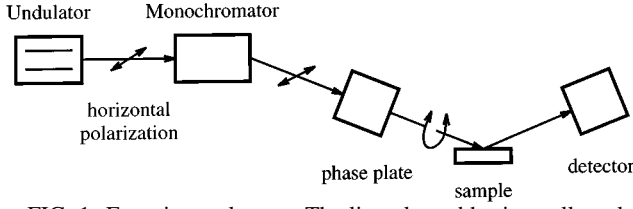


FIG. 1. Experimental setup. The linearly and horizontally polarized radiation from a planar undulator is monochromatized at 10.44 keV and then transformed into left- and right-handed circular polarization with the help of a diamond phase plate. The sample under investigation is a holmium single crystal mounted in a four-circle diffractometer and cooled to  $T=38$  K. A standard scintillation detector mounted on the  $2\theta$  arm of the diffractometer is used as the detector.

shown in Fig. 1. The magnetic gap of the planar 46 mm undulator was set to 23.40 mm and the (111) reflection from a diamond in horizontal asymmetric Laue geometry was set to accept photons of 10.44 keV. The degree of linear polarization for this setup is  $P'_\zeta = -0.97$ .<sup>7</sup> A second thin diamond crystal [0.77 mm thick and cut parallel to the set of (111) planes] was installed downstream of the monochromator and operated in quarter-wave plate (QWP) mode.<sup>5</sup> The Bragg angle for this crystal was  $16.7^\circ$  and the effective thickness crossed by the beam was 2.7 mm, with a transmission coefficient of  $1/6$ . The scattering plane of the QWP is inclined by  $45^\circ$  relative to the horizontal polarization of the incident beam, so that its  $\sigma$  and  $\pi$  components are equal. In order to transform the linear and horizontal polarization of the undulator into circular polarization by birefringence, the scattering angle of the crystal has to be slightly offset (here  $0.014^\circ$ ), from the (111)-Bragg reflection. The phase difference between the two amplitudes, which must be  $\pi/2$  for a QWP ( $\pi$  for a half-wave plate), is inversely proportional to the offset.

The degrees of linear ( $P_\zeta$ ) and circular ( $P_\eta$ ) polarization are defined as

$$P_\zeta = \frac{I_h - I_v}{I_h + I_v}, \quad P_\eta = \frac{I_r - I_l}{I_r + I_l}, \quad (1)$$

with the four intensities  $I_h, I_v, I_r, I_l$  having linear horizontal and vertical as well as circular right-hand and left-hand polarization, respectively. We call  $P'_\zeta$  the degree of horizontal polarization as delivered by the undulator and the monochromator, and  $P_\zeta, P_\eta$  the degrees of polarization obtained after the phase plate. In the following, the same notation  $I'_x, I_x$  will designate the intensities in polarization state  $x$  before and after the phase plate.

In these experiments the degree of circular polarization produced by the QWP is inferred from the measurement of the degree of linear polarization. The degree of linear polarization was determined by either using a powder diffraction polarimeter<sup>5,8</sup> or by measuring the intensity scattered by a kapton foil, at  $90^\circ$  in the vertical direction, which is essentially proportional to the horizontally polarized intensity. Due to the background scattering and to the aperture of the detector, the degrees of polarization are underestimated by the latter method. A value for the circular polarization in the QWP setting of the phase plate is obtained by comparing the

horizontally polarized intensity measured for the plate set far from the Bragg reflection [in zero-wave plate (ZWP) condition] with the intensity when set at the half-wave plate position (HWP).  $R$  is defined as the ratio of both intensities:

$$R = \frac{I_h(\text{HWP})}{I_h(\text{ZWP})}. \quad (2)$$

These intensities are corrected by the absorption of the plate so that we may replace  $I_h(\text{ZWP})$  by  $I'_h$  in Eq. (2). The depolarizing effects coming from angular and spectral dispersion of the incident beam are discussed in Appendix A. Assuming that this beam does not contain any other polarization states than linear horizontal, we can estimate the degree of circular polarization for the QWP as

$$P_\eta = \frac{1}{16} [1 + 15P'_\zeta - (1 + P'_\zeta)R]. \quad (3)$$

With  $P'_\zeta = -0.97$  and  $R = 0.063$  (measured) we determined the degree of circular polarization to be 96% for the setup of this experiment.

The sample under investigation was a single crystal of holmium ( $9 \times 4 \times 4$  mm<sup>3</sup>), with one surface cut perpendicular to the crystallographic  $c$  axis. The crystal structure of holmium is hexagonal closed packed. Below the Néel temperature of  $T_N = 131.5$  K, the magnetic moments (saturation moment of  $10.3 \mu_B$  per atom) order in a spiral with a period which in general is incommensurate with the crystal lattice.<sup>2</sup> Within the basal planes, the magnetic moments are ordered ferromagnetically. From one plane to the other, the direction of the magnetic moment is turned by a constant angle. With decreasing temperature the magnetic wave vector  $\tau$ , which is proportional to the turn angle, changes from about  $\tau \sim 0.3c^*$  at 131.5 K to  $\tau \sim \frac{1}{6}c^*$  at 20 K. Below  $T_c = 20$  K the magnetic moments are tilted out of the  $ab$  planes by about  $10^\circ$  and form a conical magnetic structure with a net moment along the  $c$  direction.

The crystal was mounted in a displex type cryostat and installed in the four-circle diffractometer with the  $c$  axis lying in the horizontal scattering plane. The mosaic width of the crystal as determined by the full width at half maximum of the rocking curve at the (002) reflection was  $0.02^\circ$ . All data were taken at  $T = 38$  K. The scattered intensity was measured with a standard scintillation detector. The incident intensity was monitored by an ion chamber located upstream of the phase plate. On-line monitoring of the degree of circular polarization was performed with a scintillation counter recording the  $90^\circ$  scattering from a  $80 \mu\text{m}$  kapton foil sitting downstream of the phase plate.

### III. CROSS SECTION AND EXPERIMENTAL RESULTS

The nonresonant magnetic scattering cross section for a single basal plane spiral is given<sup>1</sup> by

$$\begin{aligned} \frac{d\sigma}{d\Omega} = & C \sin^2 2\theta \{ \Phi_s^2 + 2 \sin^2 \theta (\Phi_l + \Phi_s)^2 + (2 \sin^2 \theta \Phi_l + \Phi_s)^2 \\ & - 4P_\zeta [\sin^2 \theta \Phi_l (\sin^2 \theta \Phi_l + \Phi_s)] \\ & \mp 4P_\eta \sin \theta (\Phi_l + \Phi_s) (\sin^2 \theta \Phi_l + \Phi_s) \}. \end{aligned} \quad (4)$$

Here,  $C$  is a constant which is independent of the Bragg angle  $\theta$ .  $\Phi_l$  and  $\Phi_s$  are the Fourier transforms of the ionic form factors (assumed to be real) of the orbital and spin magnetization densities, respectively, given in the dipole approximation. Their dependence on the scattering vector  $Q$  will be discussed in Appendix B.  $\tau$  is the modulation wave vector and  $P_\zeta$  and  $P_\eta$  are the degrees of the incident linear and circular polarization as discussed in Sec. II. The minus-plus sign in front of  $P_\eta$  refers to the sign of the magnetic satellites,  $+\tau$  and  $-\tau$ , respectively.

The first term of this formula is independent of the degree of polarization of the incident light and is identical to that for the scattering of unpolarized light. The second term describes the contribution of linearly polarized light to the scattering amplitude. Due to the minus sign before the second term, the scattering amplitude is reduced when using incident  $\sigma$ -polarized radiation ( $P_\zeta > 0$ ) while it is enhanced for incident  $\pi$ -polarized radiation ( $P_\zeta < 0$ ). This term is neglected in the further discussion because the contribution of linearly polarized light in the experiment is negligible. We note that the first two terms are independent of the sign of the magnetic satellite. The third term describes the contribution of the circular polarization to the scattering amplitude. Its sign ( $-$  or  $+$ ) depends on the helicity of the circularly polarized light in the same way as on the sign of the magnetic satellite. The scattered intensity of a magnetic satellite reflection is therefore changed by twice this term upon flipping the helicity of the incident circular polarization. The scattering amplitude is also modulated by twice this term when switching from the  $-\tau$  to the  $+\tau$  satellite, if the corresponding small changes in  $\theta$  and  $\Phi_{l,s}$  are neglected. A quantitative analysis of the integrated intensities taken at different satellites and with right- and left-hand circular polarization will therefore allow the determination of the distribution of domains with different helicities.

Figure 2 shows the magnetic scattering intensities for left ( $-P_\eta$ ) and right ( $+P_\eta$ ) handed circularly polarized light as a function of the deviation  $\phi$  from the Bragg angle ( $\phi := \theta - \theta_B$ ). They were recorded at  $T = 38$  K ( $\tau = 0.202$ ) by rocking the crystal at the magnetic satellite reflections.

Several qualitative features of the cross section are immediately apparent in the data. For both left (left column) and right (right column) handed circularly polarized light the peak intensity tends to increase with increasing scattering vector, reflecting the  $\sin^2 2\theta$  dependence of the cross section [Eq. (4)]. [The decrease in intensity expected from the decrease of the magnetic form factor with momentum transfer begins to manifest itself at the  $(006)^\pm$  and higher satellites at these incident photon energies ( $E = 10.44$  keV).] The intensity of the negative satellites  $(004)^-$  and  $(006)^-$  appears to be enhanced for right-handed circular polarization and reduced for left-handed circular polarization, as expected from the cross section. On the other hand, we see from Fig. 2 that the  $(002)^+$  satellite is slightly more intense for left-handed circular polarization (left column) compared to the right-handed circular polarization (right column). The same behavior, but with more pronounced differences in the peak intensities, is observed for the two other positive satellites, i.e.,  $(004)^+$  in the middle and  $(006)^+$  in the top of the figure. Summarizing, the peak count rates are higher for right (left) handed circular polarization at the  $-\tau$  ( $+\tau$ ) satellites and lower for the two

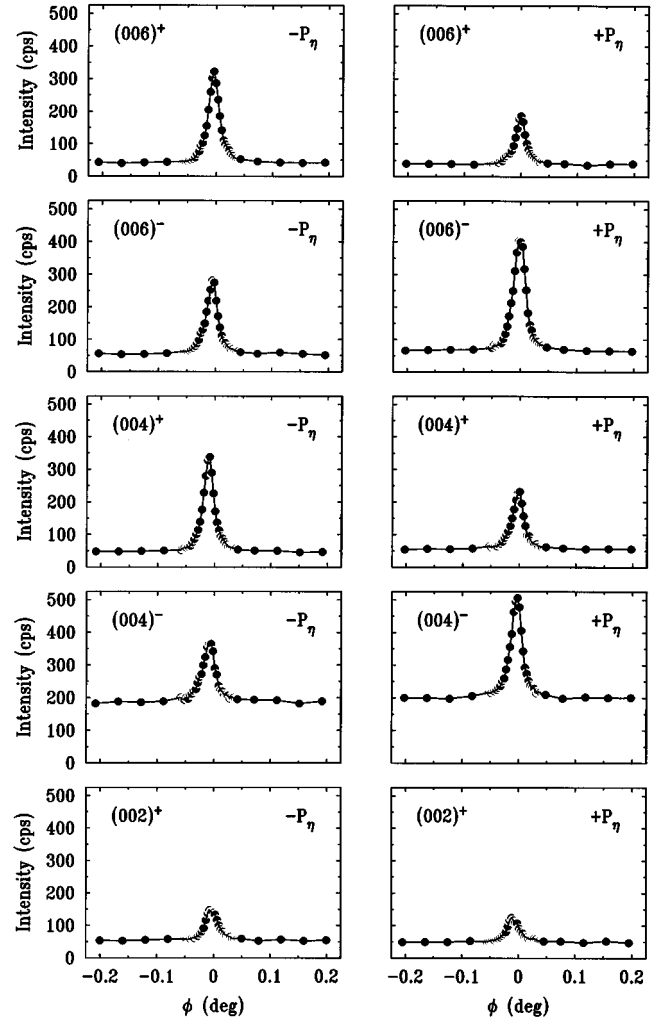


FIG. 2. Rocking scans of the five magnetic satellite reflections  $(002)^\pm$ ,  $(004)^\pm$ , and  $(006)^\pm$  of holmium at  $T = 38$  K for incident left ( $-P_\zeta$ ) and right ( $+P_\eta$ ) handed circularly polarized x rays.

opposite cases. The maximum intensity for one degree of circular polarization (vertical columns) alternates when going from one satellite to the next one, i.e., when regarding the  $+P_\eta$  column, the maximum intensity for the  $+\tau$  satellite is always lower than for the  $-\tau$  satellite. The opposite behavior is observed for the  $-P_\eta$  column. This behavior is not observed with linearly polarized light and reflects the polarization dependence of the cross section for circularly polarized x rays.

All scans exhibit comparable peak widths ( $\sim 0.02^\circ$ ) and similar background levels except for the  $(004)^-$  satellite, which is contaminated by an increased background. These high background levels have also been seen in scans along the reciprocal  $L$  direction through the magnetic satellite position and in experiments carried out with linear polarization. To explore its characteristics further, we have performed rocking scans at positions slightly off the magnetic satellite position at  $(00L + 0.02)$  and  $(00L - 0.02)$  with  $L = 4 \pm \tau$ . At these two positions the rocking scans show flat horizontal curves with no maxima lying about 50c/s above  $(00L + 0.02)$  and 30c/s below  $(00L - 0.02)$  the background level of the  $(00L)$  rocking curve. The origin of this background is un-

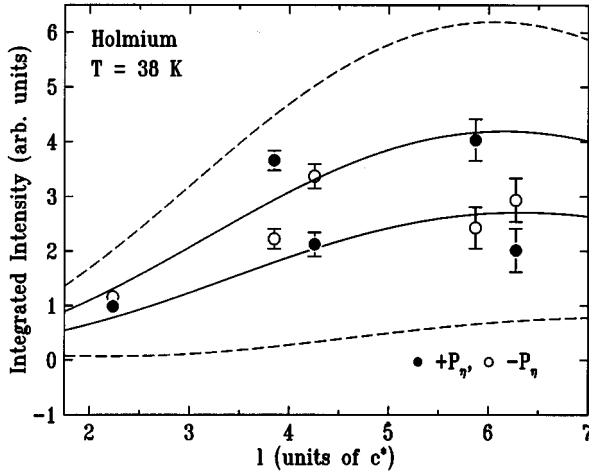


FIG. 3. Integrated intensities of the magnetic satellite reflections for left- (○) and right- (●) handed circular polarization. The dashed lines are fits of Eq. (4) to the data assuming a simple magnetic domain with positive or negative helicity. The full lines are fits of the modified equation (4) (see text) to the data assuming a distribution of magnetic domains with opposite helicity.

known. Because of its flatness in the region of the peak, it should not affect the analysis of the data.

For a quantitative analysis, the transverse line shapes were fitted to the sum of a Gaussian and Lorentzian (pseudo-Voigt) function including the linear background term  $I_b + I_s\phi$ :

$$I = I_b + I_s\phi + I_g e^{-4 \ln 2 (\phi^2/\delta^2)} + I_l \frac{\delta^2}{4\phi^2 + \delta^2}. \quad (5)$$

$\phi$  is the deviation from the peak position,  $\delta$  is the full width at half maximum (FWHM) of the peak, and  $I_g, I_l$  are the amplitudes of the Gaussian and Lorentzian functions, respectively. The integrated intensity  $A$  can then be calculated from the amplitudes  $I_g, I_l$  and the width  $\delta$  with the appropriate prefactors as

$$A = \frac{1}{2} \delta (I_g \sqrt{\pi/\ln 2} + I_l \pi). \quad (6)$$

The integrated intensities determined by the fits of the transverse scans are shown in Fig. 3 as a function of the scattering vector in units of  $c^*$ . The open (full) circles represent the data for incident left (right) circularly polarized light.

The data points show the expected qualitative behavior: The integrated intensities of the negative satellites taken with right-handed circular polarization (filled circles) are always higher than for the positive satellites. For left-handed circular polarization (open circles) the opposite behavior is observed. The difference in the intensities at one magnetic satellite for right- and left-handed circular polarization is determined by the circular polarization term in Eq. (4).

The upper and lower dashed lines in Fig. 3 show the results of a fit of Eq. (4) to the data assuming a single magnetic domain,  $P_\eta = \pm 0.96$ , and varying the constant  $C$  as the only fit parameter. The Lorentz factor  $L = (\sin 2\theta)^{-1}$  and the  $Q$  dependence of  $\Phi_l$  and  $\Phi_s$  (see Appendix B) have also

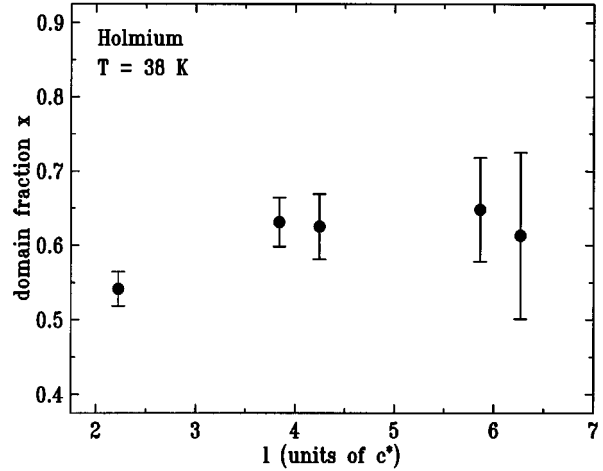


FIG. 4. Fraction  $x$  of magnetic domains with opposite helicity of the magnetic spiral as calculated from the difference in the scattered intensities at each magnetic satellite position.

been taken into account. For  $Q=0$ , the ratio of the atomic spin and orbital magnetization densities was  $\Phi_l(0)/\Phi_s(0)=3$ , as inferred from Refs. 2 and 9. The quality of the fit is relatively poor indicating either a drastic reduction in the degree of circular polarization or the existence of more than two types of magnetic domains with opposite helicity. The first explanation can be excluded because only unphysically small values of  $P_\eta \sim 0.2$  would be compatible with the data. We therefore have to conclude that more than one magnetic domain contributes to the scattering and Eq. (4), which is strictly valid only for one magnetic domain with positive helicity (the magnetical spiral turns clockwise in the coordinate system defined in the paper by Blume and Gibbs<sup>1</sup>) fails to describe the data. A spiral domain of opposite helicity can be taken into account by changing the sign before the circular polarization term. The coexistence of several domains with opposite helicity can then be included within a simple model by replacing  $P_\eta$  in Eq. (4) by  $P_\eta(2x-1)$ , where  $x$  is the domain fraction.  $x=1$  describes a single domain with positive helicity and  $x=0$  a domain with negative helicity. For equally distributed domains with opposite helicities ( $x=1/2$ ) the contribution of circular polarization to the scattering amplitude as described by the third term in Eq. (4) is zero and the only contribution is due to the first term, which is independent of the degree of polarization of the incident beam.

The solid lines in Fig. 3 are the results of the fit of the modified equation (4) with  $C$  and  $x$  as parameters, and  $P_\eta = \pm 0.96$ . The results of a fit taking into account the domain fraction  $x=0.64$  are shown as solid lines in Fig. 3. As can be seen the simple domain-fraction model allows a reasonable description of the data and establishes the existence of at least two domains with opposite helicity in the sample. There remain quantitative deviations from the theoretically expected behavior, especially for the  $(004)^-$  and the  $(006)^+$  satellites. Possible explanations for these differences are, e.g., changes in the beam footprint on the sample and small differences in the absolute beam position on the sample surface for different  $Q$  values. These can result in changes in the scattering amplitude which is dependent on the domain

distribution illuminated by the incident beam.

The domain fraction  $x$  was also calculated for each satellite reflection from the difference in the scattering intensities obtained from opposite helicities of the circular incident polarization. The results are shown in Fig. 4. The average of the calculated domain fractions  $x$  is  $0.6 \pm 0.1$ . The value for the  $(002)^+$  satellite is slightly smaller, probably due to the  $\sim 2$  times larger footprint on the sample compared to the  $(006)^+$  satellite. This interpretation could imply the existence of magnetic domains with sizes comparable or slightly smaller than the illuminated sample area thus allowing a deviation from the statistically expected domain fraction of  $x=0.5$ . We have no independent information on the domain size in the sample under investigation but note however that domain sizes of 0.1 mm to several millimeters have been observed in neutron topography measurements<sup>6</sup> and domain fractions from  $x=1/2$  to  $2/3$  have been reported in these experiments.

#### IV. CONCLUSION

In this experiment we have shown the feasibility of using a circularly polarized x-ray beam in a nonresonant magnetic scattering experiment to measure the helicity of spiral magnetic domains. A thin diamond crystal phase plate was used in quarter-wave mode to efficiently transform the linearly polarized radiation of an undulator into right- and left-handed circular polarization ( $P_\eta = \pm 0.96$ ). A quantitative analysis of the measured magnetic scattering intensities of the spiral antiferromagnet holmium shows the existence of magnetic domains with opposite helicity in the sample under investigation. X-ray magnetic scattering studies of spiral magnetic structures using circularly polarized light therefore yield information both about the magnetic structure as well as details of the distributions of magnetic domains. By using two-dimensional detectors with a reasonable spatial resolution or by scanning the sample with a sufficiently small incident beam, magnetic domains with sizes down to about 10  $\mu\text{m}$  might be detectable and yield complementary information to Kerr effect and neutron topography measurements.

#### ACKNOWLEDGMENTS

We gratefully acknowledge Professor Lang and Dr. M. Moore for the loan of the diamond crystal as well as Rose-Marie Galera for the loan of the displax cryostat. Work performed at Brookhaven is supported by the U.S. DOE, Division of Materials Science under Contract No. DE-AC02-76CH00016.

#### APPENDIX A: DEPOLARIZATION EFFECTS

Depolarization effects occur when an x-ray beam passes through a phase plate, because of the spectral and angular spread of the radiation and the nonuniform thickness of the plate. The former spreads are usually dominant and both act in the same manner. They will be represented by a single equivalent angular dispersion  $\sigma_{\Delta\theta}$  ( $\Delta\theta$  is the angular offset of the beam relative to the Bragg position). Let  $\phi$  be the phase difference produced by the plate between the  $\sigma$  and  $\pi$  component. Since  $\phi$  is inversely proportional to  $\Delta\theta$ ,

$$\sigma_\phi = \phi \frac{\sigma_{\Delta\theta}}{\Delta\theta} \quad (\text{A1})$$

and this results in

$$\sigma_\phi(\text{HWP}) = 4\sigma_\phi(\text{QWP}) \quad (\text{A2})$$

for the same  $\sigma_{\Delta\theta}$ . Such a spread in  $\phi$  produces in turn a ‘‘depolarization rate’’  $\varepsilon$  which, in the case of the HWP, we define as

$$P_\zeta(\text{HWP}) = -(1 - \varepsilon_{\text{HWP}})P'_\zeta. \quad (\text{A3})$$

When neglecting the absorption in the plate (by using a suitable normalization)

$$I_h + I_v = I'_h + I'_v, \quad (\text{A4})$$

we can write

$$\begin{aligned} I_h(\text{HWP}) &= \left(\frac{\varepsilon_{\text{HWP}}}{2}\right)I'_h + \left(1 - \frac{\varepsilon_{\text{HWP}}}{2}\right)I'_v, \\ I_v(\text{HWP}) &= \left(1 - \frac{\varepsilon_{\text{HWP}}}{2}\right)I'_h + \left(\frac{\varepsilon_{\text{HWP}}}{2}\right)I'_v. \end{aligned} \quad (\text{A5})$$

Making the assumption that the incident beam does not contain any circular or inclined linear polarization, we may calculate  $\varepsilon_{\text{HWP}}$ . If the outphase differs from the ideal phase  $\pi$  by  $\delta\phi$ , one gets for the intensities

$$\begin{aligned} I_h(\text{HWP}) &= \frac{1 - \cos\delta\phi}{2}I'_h + \frac{1 + \cos\delta\phi}{2}I'_v, \\ I_v(\text{HWP}) &= \frac{1 + \cos\delta\phi}{2}I'_h + \frac{1 - \cos\delta\phi}{2}I'_v. \end{aligned} \quad (\text{A6})$$

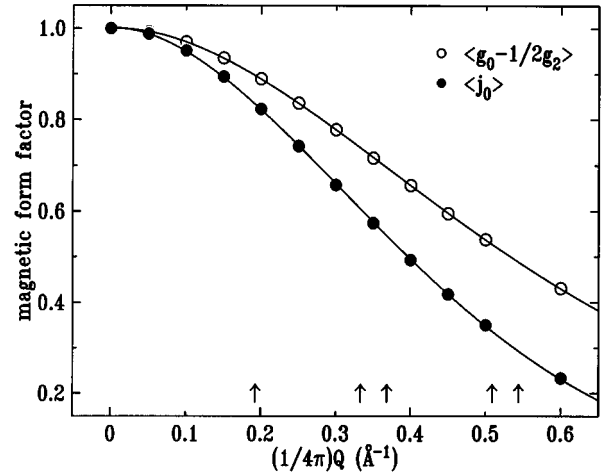


FIG. 5. Magnetic form factors for the orbital  $\langle g_0 - \frac{1}{2}g_2 \rangle$  and spin  $\langle j_0 \rangle$  magnetization densities. The arrows mark the position of the magnetic satellites  $(002)^+$ ,  $(004)^+$ , and  $(006)^+$  of holmium for  $E=10.44$  keV. The solid lines are polynomial fits of order 4 to the data.

By averaging  $\delta\phi$  over a small spread of variance  $\sigma_\phi$ (HWP) (A5) and (A6) give

$$\varepsilon_{\text{HWP}} = \frac{\sigma_\phi(\text{HWP})^2}{2}. \quad (\text{A7})$$

In the case of a QWP similar equations can be defined by replacing the ‘‘HWP’’ indices by ‘‘QWP’’ in (A5), (A6), and (A7) and defining the outphase as  $\delta\phi = \phi - (\pi/2)$ . From Eqs. (A2) and (A7) it follows that the depolarization rate for the QWP is 16 times smaller than for the HWP. Some algebra yields the degree of circular polarization in the form of Eq. (3) as a function of the quantities obtained in the experiment [ $P'_\zeta$  and  $R = I_h(\text{HWP})/I'_h$ ].

#### APPENDIX B: $Q$ DEPENDENCE OF $\Phi_L$ AND $\Phi_S$

Because of the spatial extent of the atomic spin and orbital magnetization densities, their Fourier transforms  $\Phi_s$

and  $\Phi_l$  are functions of the scattering vector  $Q$ . Using the calculations of Blume *et al.*<sup>10</sup> for the magnetic form factors of the spherical part of the spin  $\langle j_0 \rangle$  and orbital  $\langle g_0 - \frac{1}{2}g_2 \rangle$  magnetization densities one can write

$$\Phi_l = \Phi_l(Q=0)\langle g_0 - \frac{1}{2}g_2 \rangle, \quad \Phi_s = \Phi_s(Q=0)\langle j_0 \rangle. \quad (\text{B1})$$

The  $Q$  dependencies of the functions  $\langle j_0 \rangle$  and  $\langle g_0 - \frac{1}{2}g_2 \rangle$  are tabulated<sup>10</sup> for most of the rare earth elements, but unfortunately not for holmium. To estimate the magnetic form factors for holmium we follow a proposition of the authors and use the average of the form factors of the neighboring elements dysprosium and erbium. The respective values for  $\langle j_0 \rangle$  and  $\langle g_0 - \frac{1}{2}g_2 \rangle$  are plotted in Fig. 5 as a function of the scattering vector.

<sup>1</sup>M. Blume and D. Gibbs, Phys. Rev. B **37**, 1779 (1988).

<sup>2</sup>D. Gibbs, G. Grübel, D. R. Harshman, E. D. Isaacs, D. B. McWhan, D. Mills, and C. Vettier, Phys. Rev. B **43**, 5663 (1991).

<sup>3</sup>D. B. McWhan, C. Vettier, E. D. Isaacs, G. E. Ice, D. P. Siddons, J. B. Hastings, C. Peters, and O. Vogt, Phys. Rev. B **42**, 6007 (1990).

<sup>4</sup>D. N. Timms, E. Zukowski, M. J. Cooper, D. Laundry, S. P. Collins, F. Itoh, H. Sakurai, T. Iwazumi, H. Kawata, M. Ito, N. Sakai, and Y. Tanaka, J. Phys. Soc. Jpn. **62**, 1716 (1993).

<sup>5</sup>C. Giles, C. Malgrange, J. Goulon, F. de Bergevin, C. Vettier, A. Fontaine, E. Dartyge, S. Pizzini, F. Baudelet, and A. Freund,

Rev. Sci. Instrum. **66**, 1549 (1995); C. Giles, C. Vettier, F. de Bergevin, C. Malgrange, G. Grübel, and F. Grossi, *ibid.* **66**, 1518 (1995).

<sup>6</sup>J. Baruchel, M. Schlenker, and S. B. Palmer, Non-Destr. Test. Eval. **5**, 349 (1990).

<sup>7</sup>G. Grübel, J. Als-Nielsen, and A. K. Freund, J. Phys. (France) IV **C9**, 27 (1994).

<sup>8</sup>P. Suortti and G. Materlik, J. Appl. Crystallogr. **17**, 7 (1984).

<sup>9</sup>C. Sutter, G. Grübel, D. Gibbs, C. Vettier, F. de Bergevin, and A. Stunault (unpublished).

<sup>10</sup>M. Blume, A. J. Freeman, and R. E. Watson, J. Chem. Phys. **37**, 1245 (1962).